Survival analysis of a liquefiable embankment subjected to sequential earthquakes

Christina Khalil, Fernando Lopez-caballero

Survival analysis of a liquefiable embankment subjected to sequential earthquakes

C. Khalil[a,*], F. Lopez-Caballero[a]

[a] *Universite Paris-Saclay, CentraleSupelec, CNRS, MSSMat laboratory, 91190, Gif-sur-Yvette, France*

Abstract

In practice, the performance of the structure is studied based on a seismic scenario composed of independent single earthquakes. But in real life, the structure is subjected to multiple earthquakes during its typical design working life, which will produce an evolution of damage with time. The main purpose of this paper is to quantify the liquefaction-induced damage of an embankment due to sequential earthquakes during a defined working life. Moreover, a non-parametric survival analysis is used to estimate the time (in years) until a defined damage level is reached during a specific time interval. For this purpose, a site was chosen where its seismicity and its Probabilistic Seismic Hazard Analysis (PSHA) were identified. First, a site-specific seismic analysis was assessed, that consists in finding the relation between the Intensity Measures (IM) and the Engineering Demand Parameter (EDP). Second, in order to estimate the lifetime distribution as well as the Mean Time To Failure (MTTF) of the embankment, survival functions were drawn. The used

*Corresponding author

Email addresses: christina.khalil@centralesupelec.fr@ecp.fr (C. Khalil), fernando.lopez-caballero@centralesupelec.fr (F. Lopez-Caballero)

time histories were stochastically generated from synthetic ground motion models. In this study, an elastoplastic multi-mechanism soil behavior model was used. According to the obtained results, after the sequential loading, the cumulative damage is either progressive with or without extensive damages or sudden with drastic damages. Moreover, based on the chosen ground motion model, the embankment reaches a moderate damage level before its defined working life. In addition, a numerical parametric analysis is performed in order to quantify the impact of considering (or not) the loading history and the recovery time between each ground motion on the obtained MTTF of the embankment. This study pointed out on the importance of the history of loading since it affects the overall performance of the embankment. Finally, two synthetic ground motion models were assessed in order to generalize, to a certain extent, this work.

Keywords: working life, sequential, survival analysis, liquefaction, synthetic models, elastoplastic soil behavior

1. Introduction

Seismic hazard analysis involves the quantitative estimation of the ground motion (GM) hazards of a specific area. It requires the knowledge of the geologic evidence, the fault activity, the magnitude and the historical seismicity of the studied region [30, 6]. The *Probabilistic Seismic Hazard Analysis (PSHA)* considers the uncertainties in the earthquake size, location and occurrence time. It estimates the mean frequency of exceedance of any spectral acceleration at the site [5]. The level of shaking produced from this analysis comes from the contribution of the magnitude M_w, the source-to-site dis-

tance R and often the deviation of the GM from the predicted value (ε) [5]. Given the aforementioned information, the Ground Motion Prediction Equations (GMPEs) create the relationship between the magnitude, distance, and other model parameters and the Intensity Measures (IM). In this context, the study of the non linear behavior of the structures needs a recall to a large number of acceleration time histories. In addition and for particular scenarios, available data resources are sometimes inadequate to characterize the models due to several problems (i.e. ground motions from very large magnitude earthquakes, near-fault ground motions, basin effects) [57, 37, 54, 50, 60, among others]. For this reason, artificial or synthetic earthquakes could be used. They are conducted based on several methods (i.e. stochastic ground motion model, the composite source method, among others) and are useful when real motions are not available.

In practice, structures are designed to resist the first damaging earthquake scenario [23]. But during their service life, the structures are not only exposed to a single seismic event but also to multiple or repeated earthquake shocks. Previous works in this context have been conducted on various structures like buildings or bridges [20, 49, 47, 18, 63, 48, 17, 25, 41, 24, 14, among others]. As a consequence of the later, structural damage accumulation by consecutive earthquake loading will be produced. The damage accumulation according to Iervolino et al. [25], is mainly due to two phenomena: i) continuous deterioration of the material which is called "*aging*" or ii) cumulative damage due to repeated load, also known as "*sequential earthquakes*". The cumulative damage of the structure during its working life, is known as the *Life Cycle* of the structure [62, 52, 49, 25, 46, 51, 33, among others]. In

another context, the life cycle of the structure can take lots of definitions. It can be considered as the cycle needed for a structure to be constructed, maintained and economically valued (i.e. LCSA [26]). It can also be considered as the time length of the structure until the occurrence of an event of interest (i.e. equipment failure, damage, complex system), or in other words, the time-to-event study. The later is known as the *Survival Analysis*. It is generally defined as a set of statistical methods to analyze data that has the time of occurrence of an event of interest as the outcome. Such analysis is not a new subject in medicine precisely [21, 13, 9]. For example, it is used to validate the impact of a certain disease on different types of patients, or the occurrence of specific symptoms after a drug. Reflecting this analysis in the geotechnical field, it is, to the knowledge of the authors, still a new topic [39, 12, 15].

Otherwise, the behavior of the structure (e.g. reinforced concrete buildings) under seismic sequence loading is assessed based on the *Incremental Dynamic Analysis (IDA)*. It consists in subjecting the structural model to multiple ground motion records each scaled to different intensities [59]. Then, a limit state is considered in which the structure reaches failure when it exceeds the limits. On the other hand, previous studies in structural analysis have shown that, for mid-rise buildings, ten to twenty records are enough to have an estimation of the seismic demand [55, 59, among others]. IDA in this case, is easily applied since it does not have a large set of earthquake scenarios to draw fragility curves. Whereas in earthquake geotechnical engineering and particularly in liquefaction related problems, this approach is not enough to represent the overall response of the geo-structure due to i)

the multi-physical aspects of the soil (solid, water and air), ii) its history of loading that will affect its future behavior [56, 36] and iii) the correlation of the soil response with several intensity measures of the real seismic motions (i.e. Arias intensity, number of cycles) [11]

The present work aims to quantify numerically the liquefaction-induced damage on an embankment due to sequential earthquake loading. Following the Performance Based Earthquake Engineering (PBEE) approach, a PSHA should be conducted in which the seismicity of the site and the occurrence rate of earthquake are identified. In this work, the site of concern is located in Mygdonia, Greece. The reference to the fully probabilistic hazard analysis in this study are based on the work of Aristizábal et al. [2]. A large number of time histories was generated using stochastic simulations from synthetic ground motion models (e.g. Rezaeian and Der Kiureghian [45] and Boore [7]). Nevertheless any other stochastic models are also suitable to be used under the proposed methodology. At the beginning of this work, the induced damage was quantified based on a set of GM records without sequences similarly to a site-specific seismic analysis. Concerning the sequential analysis, the methodology adopted in this study is shown in Figure 1. Assuming that the working life of the embankment (T_{window}) is 100 years, and according to the PSHA and the catalog GM constructed for this site, the event rate of the mainshocks ($\lambda_{earthquakes}$) is 0.44 events/year. Thus, 44 acceleration time histories (N_{shocks}) should occur during this period. Then the sequential loading is obtained by a random permutation of the obtained number of mainshocks. In order to calculate the survival function ($P(\sum D(t) < D_{threshold})$), a threshold damage $D_{threshold}$) should be identified. Hence,the lifetime dis-

tribution of the embankment can be estimated as well as its Mean Time To Failure (MTTF, the expected time to failure for a non-repairable system). In this study, the survival analysis is computed based on a non parametric statistical method [27]. The main advantage behind this method is that it does not require the assumptions of a particular probability distribution (i.e. Weibull, exponential,log-logistic) of the structure's survival function. Also in this work, a numerical parametric analysis is performed in order to quantify the impact of considering (or not) the loading history and the recovery time between each ground motion on the obtained MTTF of the embankment. This study points out the importance of the history of loading since it affects the overall performance of the embankment. Finally, two synthetic ground motions models are assessed in order to generalize, to a certain extent, this work. The 2D finite element calculations were performed using the GEFDyn code [3]. For the soil behavior, an elastoplastic multi-mechanism model that takes into consideration the history of loading was used.

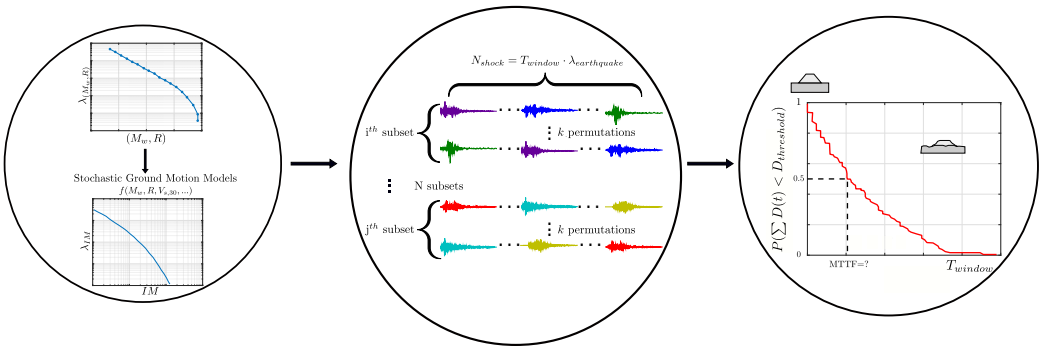

Figure 1: Schema of the used methodology to estimate the lifecycle of an embankment

The paper is structured as follows. It starts by introducing the theory behind the survival analysis in Section 2. The geometry and the numerical

model are shown in Section 3. The development of the used synthetic ground motion model is presented in Section 5. The site-specific seismic analysis of the embankment is developed in Section 6. Then, in Section 7, the sequential and the survival analysis are presented. Finally, the different types of sequential analysis approaches are developped in Section 8, as well as the consideration of different synthetic GM models. The paper is closed with conclusions.

2. Overview of the Survival Analysis

The survival analysis is the analysis of time-to-event data. These data describe the length of time until the occurrence of a well-defined end point of interest [9, 28, 53, among others]. Survival analysis is conducted via survival (or survivor) functions or hazard functions. Let T be a non-negative random variable that represents the surviving time. Denoting the duration of each event as t, the probability density function of T is $f(t)$, and its cumulative distribution is $F(t) = P\{T < t\}$. First, the survival function is:

$$S(t) \quad = \quad P\{T \geq t\} = 1 - F(t) = \int_t^{\infty} f(x)dx \tag{1}$$

The survival function is non increasing (i.e. at $t = 0$, $S(t) = 1$) and when the time increases, it tends to approach zero.

Second, the hazard function which represents the instantaneous rate of occurrence over time, is:

$$h(t) \quad = \quad \lim_{\Delta t \to 0} \frac{P(t \leq T < t + \Delta t \,|\, T \geq t)}{\Delta t} = \frac{f(t)}{S(t)} \tag{2}$$

Both, the survival and hazard functions are inversely proportional so that when the hazard increases, the survivor declines and vice versa [28, 53, among

others]. The survival time response are usually continuous. When they are not completely observed, they are called censored.

The focus of this paper is to conduct a survival analysis to find the lifetime of an embankment subjected to sequences of ground motions during a working life of 100 years. The event of interest in this case is the occurrence of these motions, which happens randomly in real life. In addition the parameters or the shape of the distribution of the embankment survival function are unknown. For these reasons, non parametric analysis will be conducted. In this section, the three methods to analyze the survival data are developed [22, 28]:

- *Non-parametric method* is a widely used method. It consists in plotting the Kaplan-Meier curve [27]. The simplicity of this curve is that it does not need any assumptions for the distribution of the survival time, or the relationship between the covariates and the survival time.

- *Semi-parametric method*, in which there is also no assumption for the distribution of the survival time but assumes the relationship between the covariates and the hazard (also the survival) function. This method uses the Cox Proportional Hazard (Cox PH) model.

- *Parametric method* assumes the distribution of the survival time and the form of the covariates.

2.1. Kaplan-Meier estimator

The Kaplan-Meier (KM) estimator (or product-limit estimator) $\hat{S}(t)$ incorporates information from censored and uncensored observations. It considers the survival function to any point in time as series of steps defined by

the observed survival and censored times [27]. The probability of surviving an event in time t_i is calculated from the probability of surviving the event at time t_{i-1}. Hence the KM estimator of the survival function is::

$$\hat{S}(t_i) \quad = \quad \prod_{t_i \leq t} [1 - \frac{d_i}{Y_i}] \quad , \tag{3}$$

with d_i is the observed cases that reached failure and Y_i is the cases that are still at risk. Normally, at $t_0 = 0$, $S(0) = 1$. Several approaches are used to calculate the variance of the KM estimator. The commonly used approach is the *delta method*. The KM estimator is viewed as a product of two proportions. Hence, in order to calculate its variance, it is better to derive one for its logarithm since the variance of a sum is simpler to calculate than the variance of a product [21]. Hence, the Greenwood formula for the variance of the survival function will be:

$$Var[S(t)] \quad = \quad Var[\exp[\ln(\hat{S}(t))] = [S(t)]^2 \sum \frac{d_i}{Y_i(Y_i - d_i)} \quad , \tag{4}$$

2.2. Cox Proportional Hazards model

The basic Cox PH model fits the survival data with the covariates z to a hazard function. Actually, this model does not directly estimate the survival functions, instead it attempts to fit it with the hazard function that has the form of

$$h(t \,|\, z) \quad = \quad h_0(t) \exp(\beta' z) \quad , \tag{5}$$

where $h_0(t)$ is the baseline hazard and β is a parameter that represents the effect of covariate on the outcome. Assuming that one event occurs at a time t_i, the parameter β can be calculated by solving the partial likelihood:

$$PL(\beta) \quad = \quad \prod_{t_i} \frac{\exp\,(\beta z(t_i))}{\sum_{j:t_j \leq t_i} \exp\,(\beta z(t_j))} \quad . \tag{6}$$

2.3. Parametric models

It is possible to estimate the survival function by making parametric assumptions. Some commonly used distributions are the Weibull (or its special case the exponential) and the log-logistic distribution. The advantages of this model is its high efficiency when it deals with small sample size. However, it is difficult sometimes to find the best distribution that fits the given data which may mislead the analysis. For more details about each distribution as well as more developed information about the survival analysis, a reference to Hosmer Jr and Lemeshow [21] is useful.

3. Geometry and Soil Numerical Model

3.1. Geometry

The model's geometry is a levee of 9 m high composed of dry dense sand. The foundation is formed of 4 m loose to medium sand (LMS) on the top of a 6 m dense sand. The bedrock is located under the dense sand. The water table starts 1 m below the surface to keep the dam dry. The inclination of the levee is a slope of 1:3 (vertical: horizontal). The geometry in this work is inspired from Rapti et al. [43], Lopez-Caballero and Khalil [34], and is detailed in Figure 2.

3.2. Soil Constitutive Model

As for the constitutive model, the *Ecole Centrale Paris (ECP)* elastoplastic multi-mechanism model (also known as *Hujeux* model) is the one chosen for this study and is written in terms of effective stress. The non-linearity of this model is represented by four coupled elementary plastic mechanism:

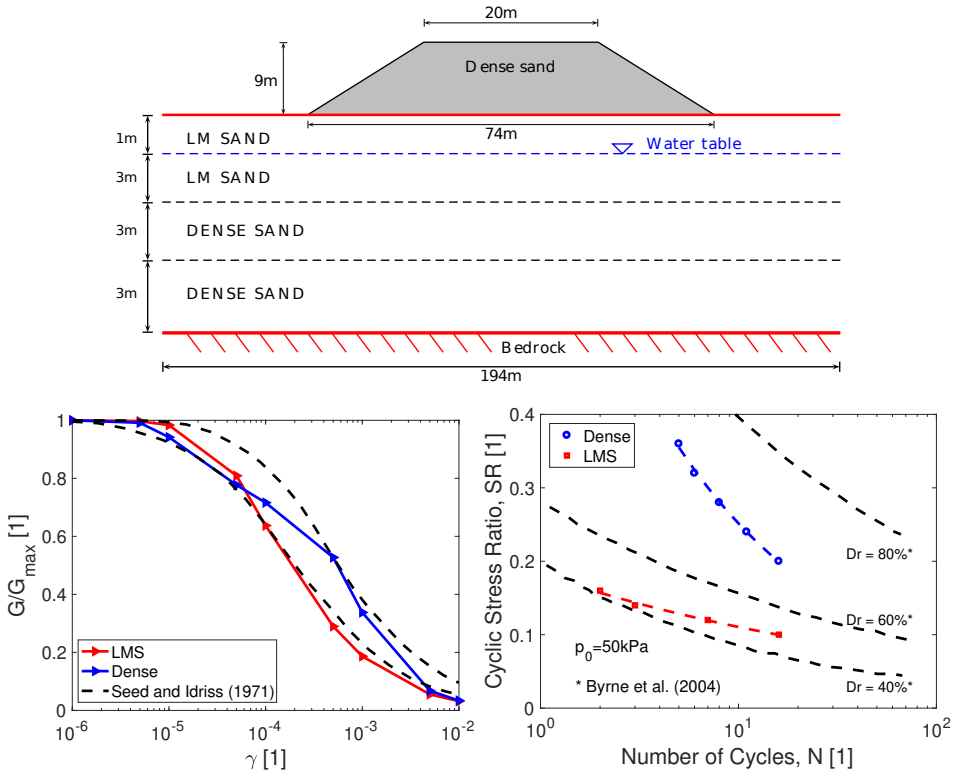

Figure 2: Geometry and behavior of the soil [34]

three plane-strain deviatoric plastic strain mechanism in three orthogonal planes (k - planes) and an isotropic plane to take into account normal forces. The model follows a Coulomb type failure criterion, contemplate the existence of dilatancy/contractancy phenomena, and use the critical state concept. The cyclic behavior is taken into account by a kinematical hardening that is based on the state variables at the last load reversal. The model is written in the concept of the incremental plasticity which divides the total strain into an elastic and a plastic part. Refer to [4, 35, 19, among others] for further details about the ECP model. For the sake of brevity only, some model definitions will be developed in the following. Considering the well-

known sign convention of the soil mechanics which sets the positive sign to the compression forces, the yield surface of this numerical model is written in the k plane as follows:

$$f_k(\sigma, \varepsilon_v^p, r_k) \;=\; q_k - \sin\phi'_{pp} \cdot p'_k \cdot F_k \cdot r_k \;, \tag{7}$$

where p'_k and q_k are the effective mean and deviatoric values of the stress tensors and ϕ'_{pp} is the friction angle at the critical state. The parameters that control the behavior of the soil are F_k, which controls the isotropic hardening associated with the plastic volumetric strain and r_k, which controls the isotropic hardening generated by the plastic shearing. These two parameters represent progressive friction mobilization in the soil. At perfect plasticity, the product $F_k \cdot r_k$ reaches unity, and the Mohr-Coulomb criterion will be satisfied. The friction angle at the critical state and F_k depends on ε_v^p such that

$$F_k \;=\; 1 - b\,\ln\left(\frac{p'_k}{p_c}\right) \;, \tag{8}$$

$$p_c \;=\; p_{c_o}\,\exp(\beta\,\varepsilon_v^p) \;, \tag{9}$$

with β is the plasticity compression modulus and p_{c_0} is the critical stress that corresponds to the initial void ratio. The parameter b shapes the form of the yield surface in $p' - q$ plane and varies between $b = 0$ where it verifies the Mohr-Coulomb criterion and $b = 1$ which will be the Cam-Clay criterion. The third variable of the yield surface which is the degree of mobilized friction angle r_k is linked to the plastic deviatoric strain $\dot{\varepsilon^p}$. It shows the effect of the shear hardening and decomposes its behavior into pseudo-elastic, hysteretic and mobilized domains. It is given by:

$$\dot{r}_k \;=\; \dot{\lambda}_k^p \frac{(1 - r_k)^2}{a} \;, \tag{10}$$

where $\dot{\lambda}_k^p$ is the plastic multiplier of k mechanism and

$$a = a_1 + (a_2 - a_1)\,\alpha_k(r_k)\;, \tag{11}$$

with,

$$\begin{aligned} \alpha_k &= 0 && \text{if } r_k^{elas} < r_k < r_k^{hys}\;, \\ \alpha_k &= \left(\frac{r_k - r_k^{hys}}{r_k^{mob} - r_k^{hys}}\right)^m && \text{if } r_k^{hys} < r_k < r_k^{mob}\;, \\ \alpha_k &= 1 && \text{if } r_k^{mob} < r_k < 1\;. \end{aligned} \tag{12}$$

Notice that a_1, a_2 and m are model parameters and r_k^{hys} and r_k^{mob} designates when the domain shows hysteresis degradation. The isotropic yield surface is assumed to be :

$$f_{iso} = |p'| - d\;p_c\;r_{iso}\;, \tag{13}$$

with :

$$\dot{r}_{iso} = \dot{\varepsilon}^p_{v_{iso}} \frac{(1 - r_{iso})^2}{c_{mon}\frac{p_c}{p_{ref}}}\;, \tag{14}$$

where d is a model parameter representing the distance between the isotropic consolidation line and the critical state line in the $(e - \ln p')$ plane and c_{mon} controls the volumetric hardening. In the model, an associated flow rule in the deviatoric k plane is assumed and the Roscoe's dilatancy law is used to obtain the increment of the volumetric plastic strain in terms of the characteristic angle ψ and a constant parameter α_ψ such that:

$$\dot{\varepsilon}^p_{vk} = \dot{\lambda}_k^p \cdot \alpha_\psi \cdot \alpha_k(r_k)\left(\sin\psi - \frac{q_k}{p'_k}\right)\;, \tag{15}$$

ψ is the characteristic angle and α_ψ a constant parameter. The density hardening is characterized by the critical stress p_c (Eq. 8) that considers all

the mechanisms (k - planes and isotropic plane). This can be related to the plastic volumetric strain such that:

$$\varepsilon_v^p = \sum_{k=1}^{3}(\varepsilon_v^p)_k + \varepsilon_v^{iso} = \frac{1}{\beta} log\frac{p_c}{p_0} \tag{16}$$

3.3. Finite Element Model

The computations were conducted by a 2D coupled FE modelling with GEFDyn Code [3], using a dynamic approach derived from the $\underline{u} - p_w$ version of the Biot's generalized consolidation theory [64]. The FE model is composed of quadrilateral isoparametric elements (3.5 m by 1 m) with eight nodes for both solid displacements and fluid pressures. An implicit Newmark numerical integration scheme with $\gamma = 0.625$ and $\beta = 0.375$ was assumed in the dynamic analysis [31]. The FE analysis is performed in three consecutive steps: i) a computation of the initial in-situ stress state due to gravity loads; ii) a sequential level-by-level construction of the embankment and iii) a sequential seismic loading analysis in the time domain. This computation is used in Section 6 and 8.1. For the computation of the sequential seismic loading developed in Section 7, and for the first motion precisely, the initial effective stresses, pore-water pressures and model history variables are stored to be used as initial state for the computation of the second ground motion. The storage of the history variable of the ith computation will be used as initial state of the ith+1 computation. More details regarding the calculation procedures are developed in each section.

3.4. Boundary Conditions

In the analysis, equivalent boundaries have been imposed on the nodes of lateral boundaries (i.e., the normal stress on these boundaries remains

constant and the displacements of nodes at the same depth in two opposite lateral boundaries are the same in all directions). They are the response of a modeled infinite semispace. Hence, only vertically incident shear waves are introduced into the domain. The model is wide enough (194 m) to ensure that the effect of the boundaries on the response of the model can be neglected and also to satisfy the free field condition at the lateral boundaries. For the half-space bedrock's boundary condition, paraxial elements simulating deformable unbounded elastic bedrock have been used [38]. The incident waves, defined at the outcropping bedrock are introduced into the base of the model after deconvolution.

4. Assumptions for this study

For the study of the life-cycle of a levee subjected to sequential signals, basic assumptions are made:

- The cumulative damage of the levee is due to the effect of the series of mainshocks only. The effect of aftershocks is not taken into account.
- The effect of aging is not considered. For example, there is no consideration of the rain or sun, the wind load or any other type of loads that may be caused from external uncontrolled conditions. Also aging needs a deeper study of the material resistance, origin and age, which are not considered in this study.
- At the beginning of the study, before the first seismic loading, the embankment is considered in its virgin and stable state. It does not have a history of earthquake loading.

- The embankment is not subjected to any repairs during its lifetime.
- The constitutive model does not take into account the secondary consolidation or compression after each seismic loading.
- The pore water pressure have dissipated after each seismic loading. It is ensured by adding a time-gap (recovery time) between each mainshock. This assumption is evaluated later in the paper.

5. Input Ground Motions

The seismicity of the site requires the knowledge of the geographical location, the site characteristic and the magnitude-frequency distribution of the earthquakes. The seismic hazard analysis involves the quantitative estimation of the ground motion characteristic at a particular site with the help of deterministic or probabilistic approaches. The *Probabilistic Seismic Hazard Analysis (PSHA)* sets a predictive relationship for each ground motion parameter in each source. This method combines the uncertainties in the earthquake characteristics to obtain the probability that any IM will be exceeded at a particular time period. The hazard curve is used to identify the ground shaking level or the mean annual rate of exceedance (λ_{IM}) [44]. Once the main aspects that characterize the local seismic hazard are defined, it is possible to proceed with the selection of time histories. For this purpose, calibrations are used to adjust recorded ground motions and make them more representative of the analysis conditions [57, 61, among others].
Concerning the present work, the response of the embankment based on sequential seismic loading is the major focus of this paper. The site of concern

is a valley in Mygdonia that has an epicentral distance located about 30 km to the NE of the city of Thessaloniki in northern Greece. The magnitude M_w in this area is between 4.5 to 7.8. The fully probabilistic hazard analysis is adopted from the study of Aristizábal et al. [2] on the same site. They generated a long catalog from 500 years to 50,000 years (equivalent to a probability of exceedance of 1% in 50 years). Hence, the magnitude-frequency distribution for 50,000 years catalog is shown in Figure 3a. More details regarding the PSHA are presented in the work of Aristizábal et al. [2].

In the case of regions with lower seismicity, it is not easy to know with a higher level of accuracy, the expected ground motion scenarios. In practice, the effect of various GMPE's is studied. In addition, to generalize (to a certain extent) this work, two synthetic ground motion models were used: Rezaeian and Der Kiureghian [45] and Boore [7]. They are designated as *Mod.R* and *Mod.B* accordingly. *Mod.R* uses an NGA database [10] and for *Mod.B*, Aristizábal et al. [2] adapted the Akkar et al. [1] GMPE which provides a good representation of the Europeen context. The hazard curve built from the generated catalog of the two synthetic ground motion model, is shown in Figure 3b. It can be seen from this figure that the 10% of exceedance for 100 years ($\lambda_{IM} = 0.001$ 1/year) is 0.2 g for *Mod.B* and 0.5 g for *Mod.R*. Concerning the methods of each model, both are based on stochastic simulations. They tend to directly simulate the recorded ground motions with varied characteristics including the variability of the ground motion [45, 61, among others]. For *Mod.R*, the method consists in rotating the recorded ground motion pairs into their principal axis and choosing only the strong component. As for *Mod.B*, the stochastic method consists

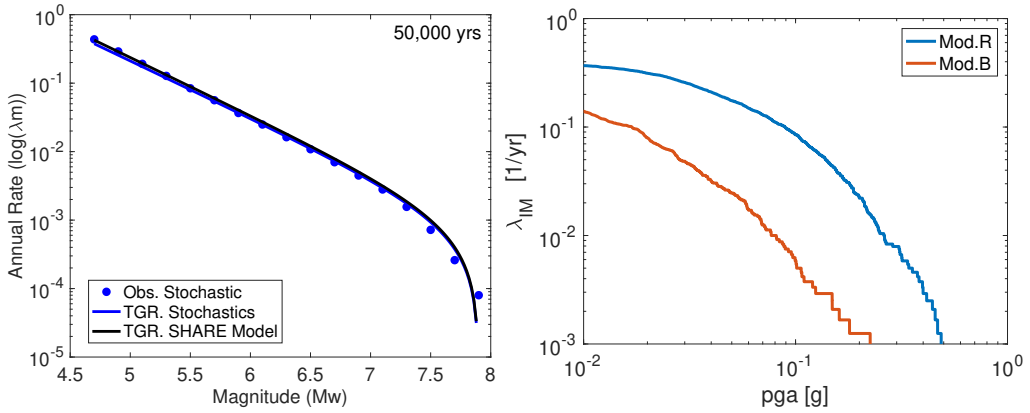

(a) (b)

Figure 3: a) The magnitude-frequency distribution curve for 50,000 years catalog [2] along with b) the PGA hazard curve of the generated synthetic ground motions

in distributing randomly the energy over a duration equal to the inverse of the low frequency corner. The different ground motion parameters can be obtained by using the random vibrating theory [8]. For the sake of brevity, the deeper details and equations of each stochastic model are omitted, it is recommended to refer to each cited paper for more information. The spectral response of the two models is drawn in Figures 4a and 4b. It is clear that the spectral acceleration of *Mod.R* is higher than *Mod.B*.

Because it is difficult to understand the complexity of the earthquakes from one parameter [30], and based on Kawase [29] there exists a proportional relation between the outcrop acceleration and the equivalent predominant frequency which is $T_{v,a} = \alpha.PGV/a_{max,out}$ with $\alpha = 4.89$. These three parameters are represented in Figure 5. PGV is represented as dashed lines. Although the two models represent the same site, they use different relationships to determine their parameters and in consequence the corresponding

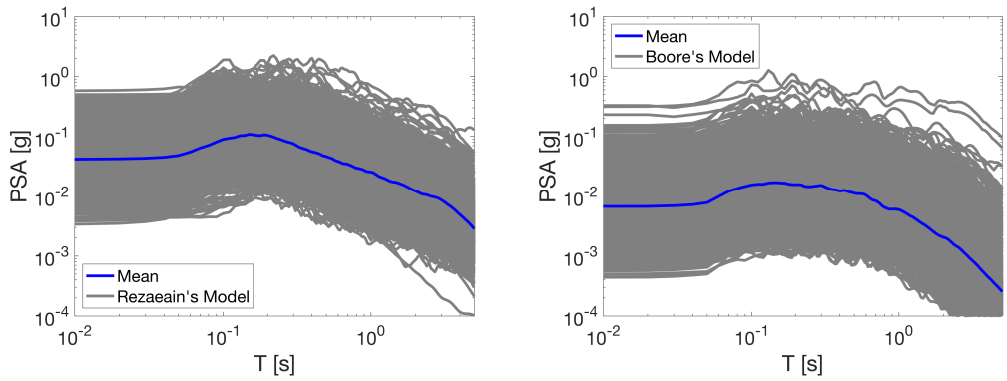

(a) (b)

Figure 4: The response spectral of a)*Mod.R* and b)*Mod.B*

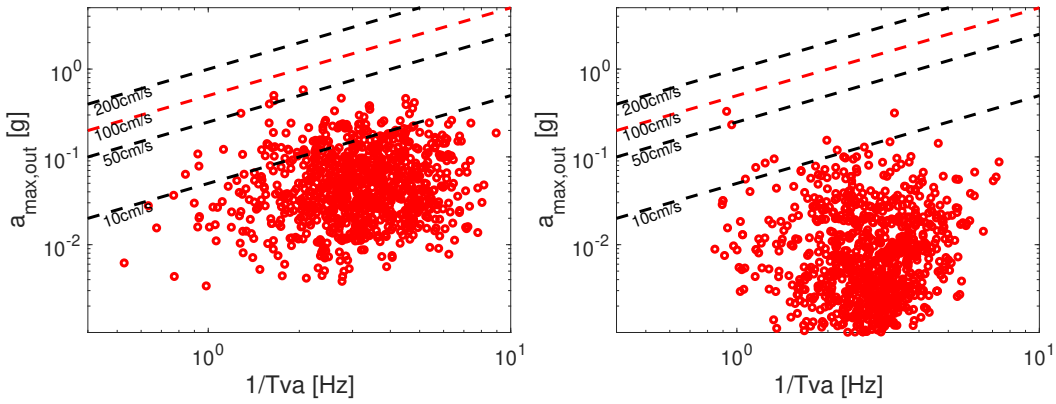

(a) (b)

Figure 5: The distribution of some ground motion parameters of the two models: a) *Mod.R* and b) *Mod.B*

IMs. This proves the difference in the results shown in Figure 5. They are compatible in their frequency interval but not in their peak acceleration; *Mod.R* has a higher acceleration than *Mod.B*. Also, the majority of the motions of *Mod.B* have a *PGV* less than 10 cm/s which is not the case for

Mod.R.

After identifying and presenting the different synthetic ground motion models used in this study, a site-specific seismic analysis will take place. The response of the embankment will be calculated after a set of unsequenced ground motion records.

6. Site-Specific Seismic Analysis

In Section 5, the used synthetic ground motions were presented. Two models were used (*Mod.R* and *Mod.B*). In this section, the response of the embankment based on each seismic load will be developed. Since the crest settlement is the mode of failure normally studied in case of embankments, it will be the parameter for the damage quantification. It is calculated by considering each ground motion as a single event. The percentage relative crest settlement as calculated by Swaisgood [58] is the ratio of the vertical displacement of the crest to the height of the dam with its corresponding foundation: $\delta u_{z,rel}/H$, given that H in this study is 19 m. The relative crest settlement is divided into damage levels [58, 34]. The limit values of these levels is still debatable but the ones chosen for this study are shown as dashed lines in Figure 6. When $\delta u_{z,rel}/H \leq 0.02\%$, there is *No* damage, if $0.02\% < \delta u_{z,rel}/H \leq 0.1\%$, the damage is *Minor*, if $0.1\% < \delta u_{z,rel}/H \leq 1\%$, the damage is *Moderate* and finally if $\delta u_{z,rel}/H > 1\%$, the damage is *Serious*. Figure 6 shows the relative crest settlement obtained using the two models: *Mod.R* and *Mod.B*. As expected and as seen in Figure 6, the relative crest settlement $\delta u_{z,rel}/H$ increases with the peak ground acceleration for both models. Since the acceleration of *Mod.R* is higher than *Mod.B* (proved in

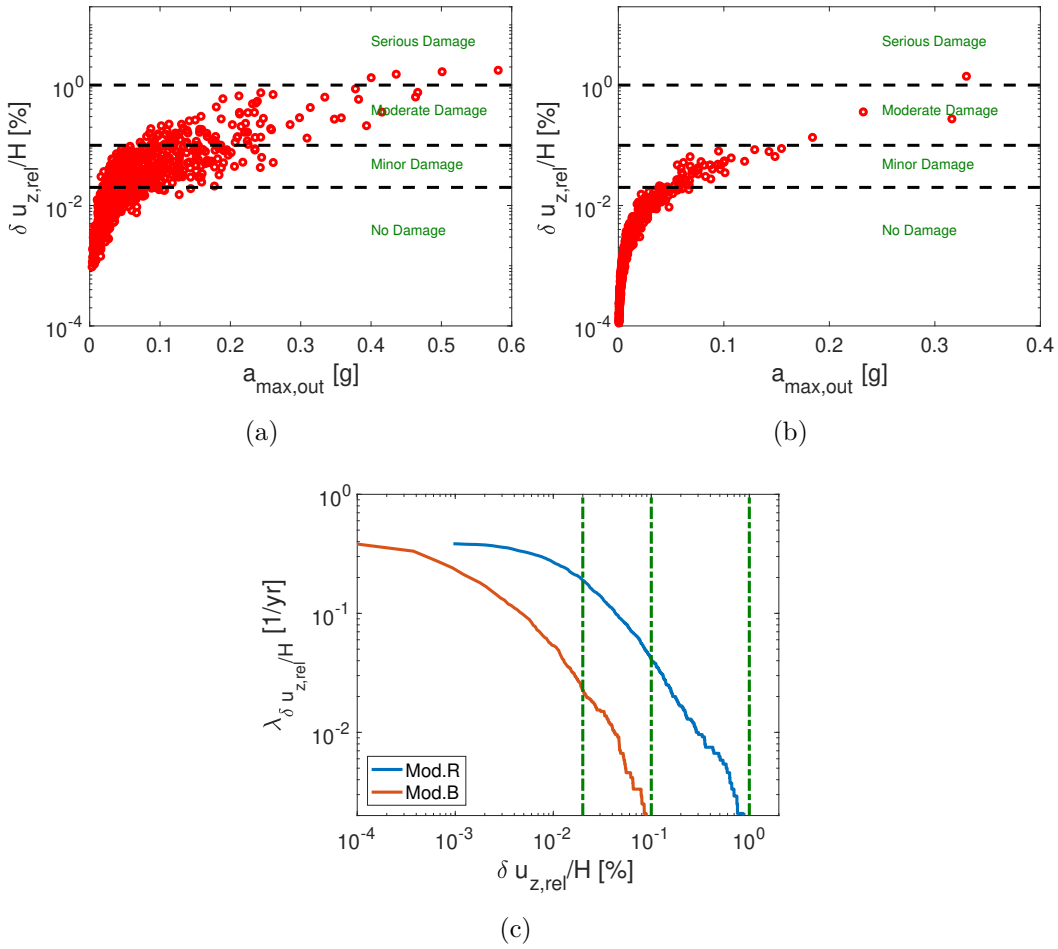

Figure 6: The variation of the crest settlement with respect to the outcrop acceleration of the two models: a) *Mod.R* and b) *Mod.B* and c) the obtained crest settlement hazard curve.

Section 5), *Mod.R* induces more damage than *Mod.B*. Comparing the damage levels, it can be seen that *Mod.B* in majority, did not show any damages; few values of $\delta u_{z,rel}/H$ were in *Minor* damage and only one shows *Serious* damage. Whereas *Mod.R* shows more variability in the damage levels that

lies in majority in *Minor* and *Major* damages. But on the contrary of Figure 6b, only four ground motions showed *Serious* damage for *Mod.R*. In addition, a hazard curve for the crest settlement was obtained using the two stochastic models (Figure 6c). The damage levels are also represented as dashed green lines in this figure. It can be seen for example that with a 10% of exceedance in 100 years, the obtained co-seismic settlement using *Mod.R* corresponds to the *Serious damage* level. Whereas for Mod.B, for the same probability, *Moderate damage* is the corresponding level.

It was seen in this section that the two synthetic ground motion models show different results in terms of the embankment performance. These results highlight the importance of the choice of the ground motion model.

7. Survival Analysis of the Levee

Also in the scope of the PBEE methodology, the lifetime of the structure is the length of time until failure occurs. In order to calculate it, the degradation of the structure over time should be considered. Thus, the study of its performance due to sequential loading is required. In Section 6, it was shown that the two synthetic ground motion models gave different responses and that *Mod.R* induced more damage. Thus, this model will be used to compute the seismic sequential loads as well as the survival life of the tested embankment. Assuming that the working life of the embankment (i.e. T_{window} in Figure 1) is 100 years, the occurrence rate of event during this life corresponds to 44 acceleration time histories (i.e. $N_{shock} = 44$) which means $\lambda_{earthquake} = 0.44$ events/year. In order to be statistically representative, a large number of subsets must be used. In this work, 21 subsets (i.e.

$N_{subset} = 21$ in Figure 1) compatible with the seismic hazard of the tested site were used. The 44 events were permuted randomly 10 times (i.e. $k = 10$ in Figure 1) for each subset. In total, 210 sequences of ground motions were created for a serviceable life of 100 years. It should be reminded that for the sequential computation, the storage of the history variable of the ith computation will be used as initial state of the ith+1 computation.

This section is divided into two parts. The first part develops the quantification of the relative crest settlement of the embankment for each sequence. The second part develops its survival analysis.

7.1. Crest settlement in the sequences

Based on Iervolino et al. [25], the damage accumulation is due to either the aging of the material or the sequential earthquakes. The first degradation model is called the deterioration-based: the system degrades progressively due to internal factors such as aging, corrosion in steel or wear [40, 42]. The second degradation model is the shock-based model where the system is subjected to a sudden decrease in its performance due to an earthquake [40, 42]. In this work, the aging is not taken into consideration because it needs a deeper understanding of the material origin, resistance and age. As explained in the introduction of this section, the event of interest is the occurrence time of different mainshocks sequences.

In order to ensure that the pore water pressure is dissipated completely after each mainshock (the sixth assumption in this study), a recovery time of 30 seconds is considered. It was chosen in a way to ensure the dissipation of Δp_w without the generation of expensive computational time. In order to validate if this recovery time is enough for the dissipation of Δp_w, one input ground

motion is considered and a post-seismic loading is applied. The results are shown for a sample located at 3 m depth under the center of the embankment (Figure 7a) and at free field (Figure 7b). It is interesting to note that after

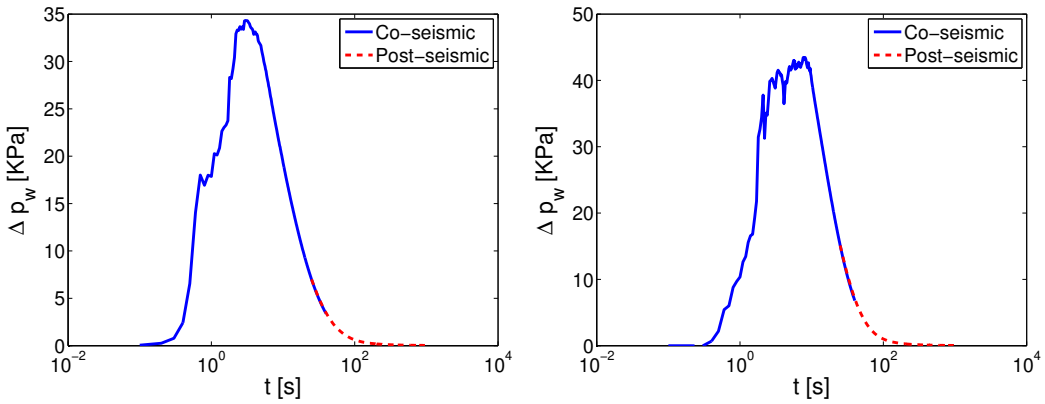

Figure 7: The excess pore water pressure of one mainshock a) under the center of the embankment and b) at free-field

the co-seismic loading, the excess pore water pressure is near zero in the two locations. The post-seismic loading, where the embankment is returned to its static case, proves that chosen recovery time can be enough since the two curves overlapped and follow the same path.

Concerning the damage quantification of each sequence, the relative crest settlement $\delta u_{z,rel}/H$ is calculated based on the method developed in Section 6. Figure 8a shows $\delta u_{z,rel}/H$ and the corresponding damage levels for all the seismic sequences. To better visualize the results and conduct the analysis, Figure 8b shows $\delta u_{z,rel}/H$ in the form of box-plots (aka Speaker style). A small explanation about this form of graph is discussed herein before proceeding in the discussion of the results. The median of the tested data is

represented by the small bars in the boxes. The boxes represent 50% of the data and there boundaries considers 25th and 75th percentile of the data respectively. The two extremes are 1.5 times the distance between the two percentiles, and the red dots above or below the box-plots are the outliers.

Back to the analysis of the relative crest settlement of *Mod.R* sequences

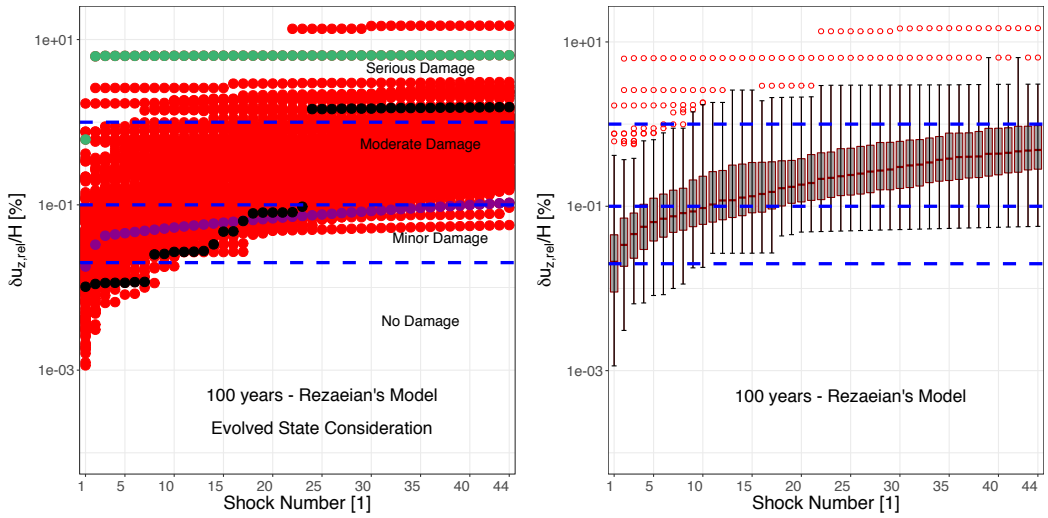

Figure 8: The relative crest settlement of the sequential signals a) for all the sequences and b) in form of box-plots

and as expected, $\delta u_{z,rel}/H$ increases when the number of shocks increases (Figures 8). Based on these results, the increment was either progressive during the sequential load, or sudden after few mainshocks. For this purpose, three curves are selected for interpretation. For example, the purple curve in Figure 8a shows that after the first shock, the embankment had *No* damage. The relative crest settlement kept increasing during this sequence but in a small manner. At the end of this sequence, the embankment

showed a damage level located in the interface between *Moderate* and *Minor* damage. This case can be considered "safe", in the point of view that the cumulative damage did not lead to failure. On the opposite, the green path shows a *Moderate* damage directly after the first shock. The embankment was not able to resist the load repetition and hence it failed drastically after the second shock till the end. For the path in black, the damage was progressive. The embankment had *No* damage until the seventh shock. After it, $\delta u_{z,rel}/H$ increased progressively until after the 23rd shock, the embankment was not able to resist and the induced damage was drastic. It should be mentioned that previously, in Section 6, only four ground motions showed *Serious* damage. The occurrence of these motions in the sequence, either led to a good densification of the soil and hence less damage or it increased the crest settlement to a severe case.

Another statistical way to visualize the results is found in Figure 8b. Based on the median value, $\delta u_{z,rel}/H$ increases with the shock increment. For the first shock, 50% of the data showed *Minor* damage. But after the 44th shock, 50% of the data showed *Moderate* damage. The upper quarter of the data showed *Serious* damage. The outliers are presented in the upper part of the graph which proves that the embankment fails completely for some cases at the beginning of the sequences. An associated explanation is also represented in Figure 9 with the empirical Complementary Cumulative Distribution (CCDF). This figure shows the distribution of the relative crest settlement after a specified number of shocks. The damage levels are also represented by blue dashed lines. For the damage line 0.1% for example, the distribution of the relative crest settlement increases when the shock

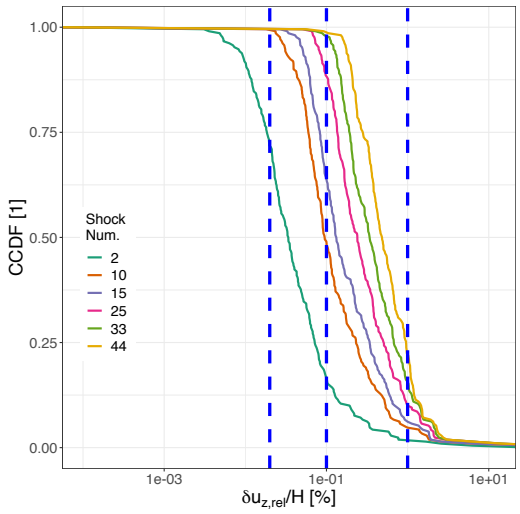

Figure 9: The complementary cumulative distribution function (CCDF) of the relative crest settlement

number increases. After the 10th shock, 50% of the tested sequences shows that the embankment will be deteriorated in a *Moderate* damage. Usually in engineering practices, the green curve in Figure 9, is similar to the ones conducted in Section 6 where the response of the embankment is calculated after the occurrence of independent earthquakes. It was shown so far in this work, that this curve can be misleading and may not represent the behavior of the embankment for a long term.

On the other hand, since the ground motions sequences are chosen for a working life of 100 years, the change in the damage levels between the years is interesting to identify. Figure 10 shows the Damage Level (DL) of the selected ground motion as function of the magnitude and the source-to-site distance. Since the acceleration time histories during the lifetime are permuted randomly, it is evident that the ground motions are not in the same

position in the first, 50 and 100 years. The damage levels are numerated from 1 to 4 to represent *No* damage to *Serious* damage respectively. From Figure

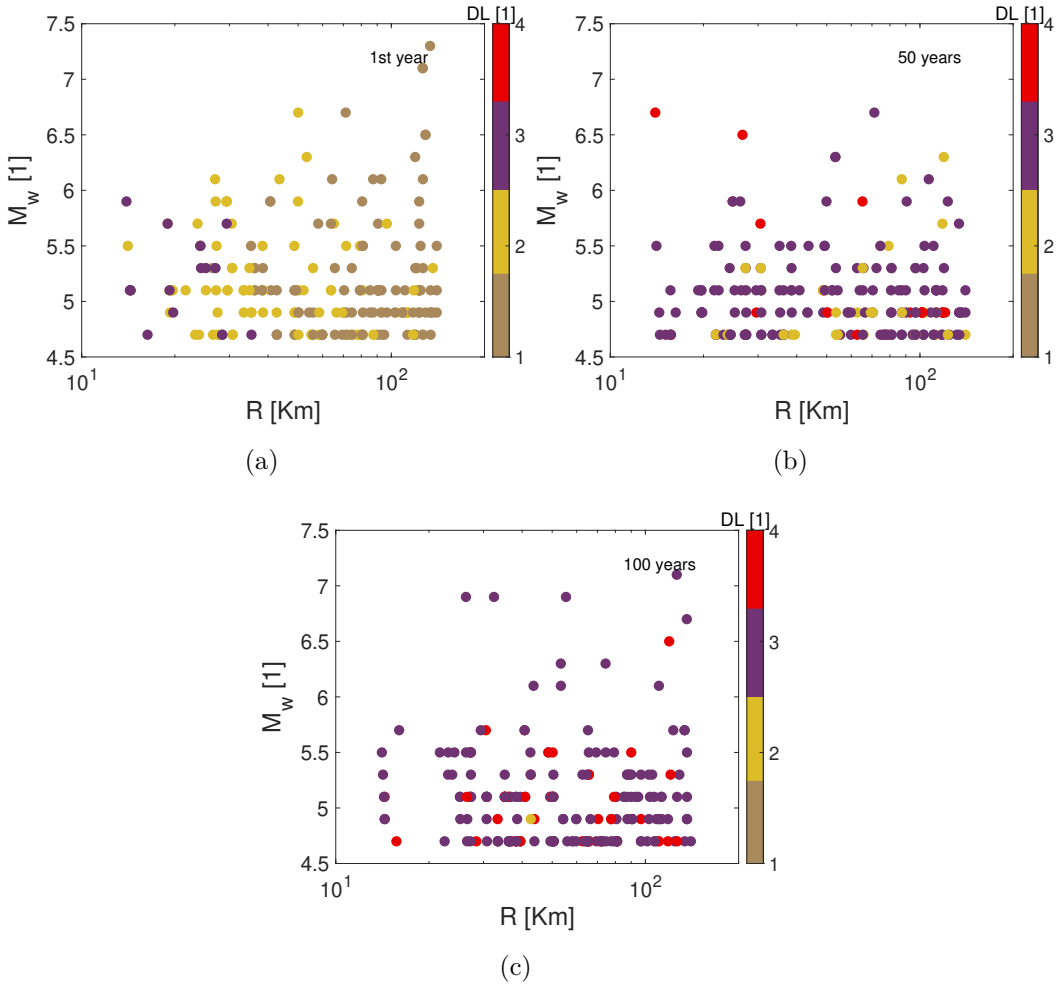

Figure 10: The damage levels of *Mod.R* with respect to the magnitude and distance of the seismic motions

10a, after the first ground motion, very few responses show damage level of class 3. The other responses were either 1 or 2. After 50 years of sequential ground motions (Figure 10b), it is clear that there is no damage level of

class 1 and very few of class 2. Finally, at the end of the chosen working life (i.e. 100 years), more damage levels of class 4 are shown (Figure 10c), which means that the embankment have a high risk to fail at the end. This synthesis is similar to the one found previously in this section with a different type of analysis.

As a partial conclusion of this section, it is noted that the loading history of the embankment will definitely affect its behavior in the long term. Even if the embankment was intact after few shocks, the failure can be reached in the working life. In addition, some sequences showed that the embankment was drastically damaged after few shocks.

7.2. Survival analysis

The survival analysis is the analysis of data involving time needed for an event of interest to happen. It is also known as the time-to-event data. Detailed explanation about this analysis were developed in Section 2. The event of interest in the scope of this study, is the occurrence of mainshocks during a working life of 100 years. For this purpose, the survival function is calculated based on the Kaplan-Meier estimator [27]. The estimated probability is usually a step function and is shown in Figure 11. The three damage levels are represented in this figure. An important quantity that can be derived from this figure, is the Mean Time To Failure (MTTF, the expected time to failure for a non-repairable system) that is also represented. After two years (i.e. MTTF = 2.27 years), 50% of the cases survived the damage level of class 2 (i.e. *Minor* damage). Whereas the MTTF of class 3 (i.e. *Moderate* damage) is 25 years. At 100 years, the survival probability of this damage level is zero. For *Serious* damage, 25% of the cases were not able to survive.

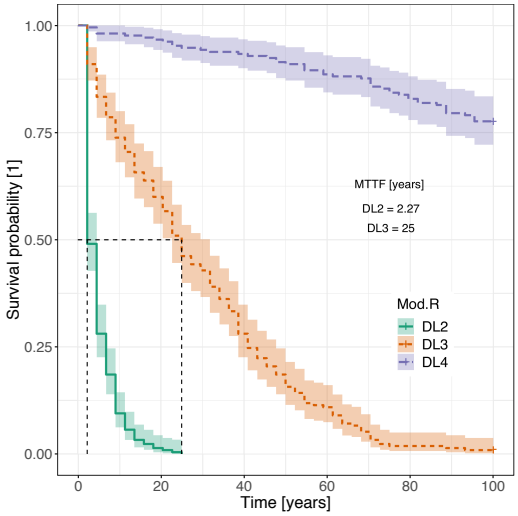

Figure 11: The survival probability of the levee for *Mod.R*

In all the preceding, the survival function was conducted based on a non parametric approach. It is important to mention that even when the parameters of the distribution are unknown, distributions such as Weibull, lognormal, exponential or others, can be fitted from results obtained from non parametric methods. The accuracy of this fitting is ensured by the Kolmogorov–Sminorv (KS) test [32]. It was carried out for each empirical distribution of the two critical damage levels. Both, the Weibull and its special case the exponential, could be considered according to the KS test. It should be noted that the distribution of the survival function in case of Weibull is $S(t) = \exp(-\alpha\, t^{\gamma})$ and in the case of exponential is $S(t) = \exp(-\lambda\, t)$. Table 1 shows the obtained parameter of each damage level from the survival function found in Figure 11. The interpretation of these results are pointing on the idea that the Weibull distribution is more appropriate to represent the slow deterioration overtime whereas the exponential distribution can be

used to represent the deterioration after sudden shocks. Since the *Moderate* damage was mainly due to the progressive increase of the crest settlement, its distribution can be approximated to follow a Weibull distribution. Whereas *Serious* damage is more likely to follow the exponential distribution because the failure was sudden in most of the cases. Thus, the results obtained for

	Weibull		**Exponential**
	α	γ	λ
With Recovery Time (Section 7.2)			
DL3	0.058	0.909	0.037
DL4	$1.9.10^{-3}$	1.057	$2.5.10^{-3}$
No Loading History (Section 8.1)			
DL3	0.065	1.344	0.014
DL4	$5.77.10^{-5}$	2.387	0.018
No Recovery Time (Section 8.2)			
DL3	0.024	1.175	0.044
DL4	$9.19.10^{-5}$	1.961	0.007

Table 1: The distribution parameters of *Moderate* and *Serious* damages for the three tested cases of this work

both distributions confirm the biases that could be introduced in a parametric approach when the survival function is not well known.

8. Influence of various parameters on the survival analysis

To this point of this article, it was represented an analysis of the relative crest settlement of an embankment after both, a single event and sequential

events of mainshocks. This later considered sequences of 44 mainshocks with a recovery time between each. In addition, the survival function was calculated based on a non parametric approach. In this section, answers on the following questions will be discussed respectively:

- What if the loading history was not considered? Technically, what will happen if the embankment was returning to its initial state after each ground motion of each sequence.
- What if there was no recovery time between the GM which means that the mainshocks are sequenced in a back-to-back form?
- How the response will differ if the analysis was conducted based on a different synthetic ground motion model (e.g. *Mod.B*)?

8.1. Effect of the loading history

In soil precisely, the history of loading plays a major role for its future behavior. Many previous studies have been conducted to check the effect of past histories on the response of geo-structures (i.e. Sica et al. [56], Lopez-Caballero et al. [36]). Moreover, it was seen in the previous section, that even if the embankment was intact after few years, it might be damaged in a long time. Its state evolves based on the years of loading. Considering now the sequences are formed by simply adding the responses found in Figure 6a based on their occurrence, Figure 12a will be obtained. Based on this figure, the results did not show too much dispersion and few oultiers, on the contrary of the results in Figure 8b. The embankment started its cycle of life with a *Minor* damage, to attend a *Serious* damage after half of its lifetime.

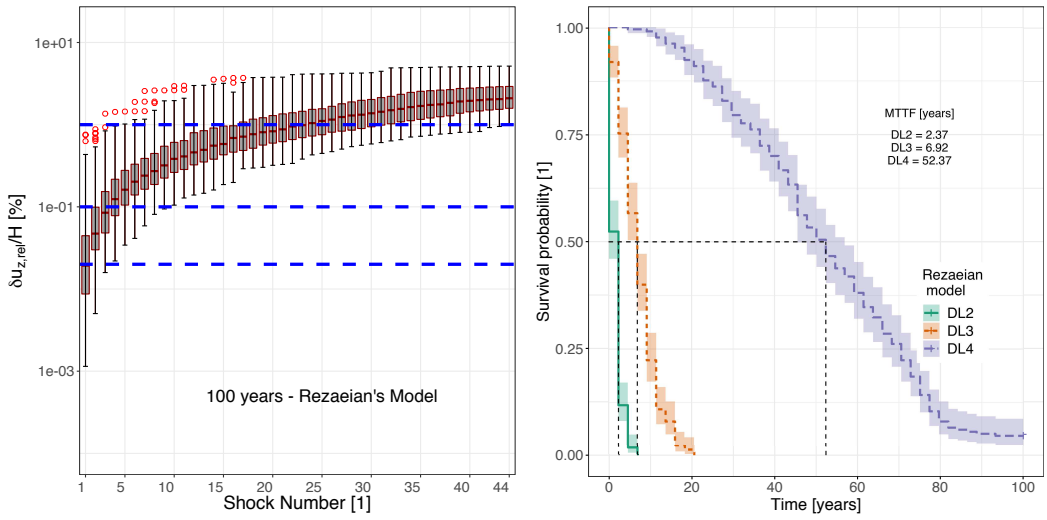

(a) (b)

Figure 12: The relative crest settlement with No loading history a) in the form of box-plot and b) its survival analysis

The difference between the response of the embankment with consideration of its evolved state (Figure 8b) and that presented in Figure 12a is that the last one over estimates the results. The embankment settles less when in its history, it was subjected to many loads: this is due to the consolidation of the soil and the evolution of its properties.

Concerning the survival analysis of this case (Figure 12b), after approximately 7 years (i.e. MTTF = 6.92 years), the embankment will moderately survive the applied sequential loads. Whereas after almost half of its serviceable life (i.e. MTTF = 52.37 years), it will be damaged drastically. These results are very different from the ones obtained in Section 7.2. The parameters of the survival function distributions are shown in Table 1.

Maybe this analysis satisfies the decision makers as they consider it "preven-

tive" for security reasons, but besides the fact that it is not realistic, it could mislead the design and may generate additional useless costs.

8.2. Importance of the recovery time between the sequences

Based on codes and literature, a system is considered to fail when its cumulative damage due to shocks exceeds its capacity of resistance [16, 25, 42, among others]. On the opposite of the structural systems, geotechnical systems have in majority, recovery times that if not considered in the analysis, it may lead to severe and over estimated damages. In this section, a comparison of the survival function of three different types of shock-based approaches is considered. The approaches are i) the consideration of the the recovery time between each shock (Section 7.2), ii) taking the shocks in a back-to-back form and iii) the consideration of the loading history (Section 8.1). The results are shown in Figure 13. The survival probability was analyzed for two damage levels: *Moderate* damage ($0.1 < \delta u_{z,rel}/H < 1$) in Figure 13a and *Serious* damage ($\delta u_{z,rel}/H > 1$) in Figure 13b.

For both damage levels, it can be seen that the loading history plays a major role in the response of the embankment: without its consideration, the relative settlement was over estimated. This over estimation may be beneficial if the region was of low seismic activity. But for some cases, it can be a result of high cost of construction/reparation. Considering the *Moderate* damage (Figure 13a) and comparing the orange and the green curves, it can be noticed that there are five years of survival life that are not taken into account if the recovery time was not ensured. In addition, it is clear, from the different values of the MTTF, that loading history has an important effect. Whereas for the *Serious* damage (Figure 13b), it is important to mention

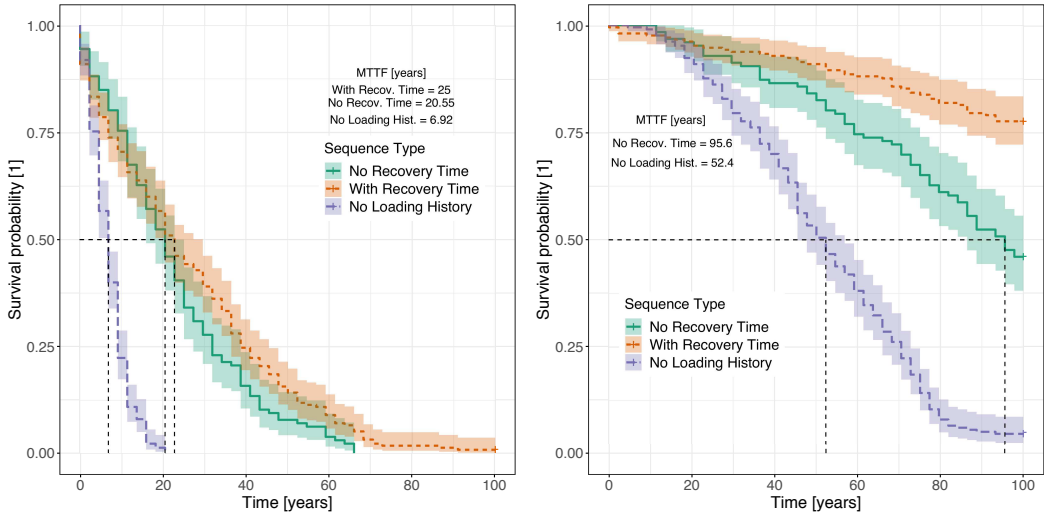

(a) (b)

Figure 13: The survival analysis of the different sequence types for a) Moderate damage and b) Serious damage

that the embankment did not reach the MTTF when the recovery time was ensured. The parameters of the survival function distribution are shown in Table 1.

8.3. Effect of different synthetic ground motion models

The survival analysis in this paper was conducted based on the synthetic ground motion model called *Mod.R* since it showed more variety in the response of the embankment and its damage level (Section 6). This section will consider *Mod.B* in a back to back form (or with no recovery time) since this type of calculations needs less computational time. Adopting the same strategy developed in this paper to calculate the survival functions, the results are obtained in Figure 14 as function of two damage levels: *Minor* damage

(DL2) and *Moderate* damage (DL3). Also in this figure, a comparison of the survival function with *Mod.R* in back-to-back form is shown. It is clear how the survival function for *Mod.B* is very optimistic and shows that the embankment is able to resist the shocks during its lifetime. At 41 years for example, there is 50% chance that the embankment will survive a damage level of DL2 if it was subjected to *Mod.B*, whereas based on *Mod.R* it needs 2 years (Figure 14a). Also for DL3, based on *Mod.B*, the embankment have high chances to survive this damage level whereas based on *Mod.R*, after 20 years, it will have only 50 % chance to survive it (Figure 14b). It is evident

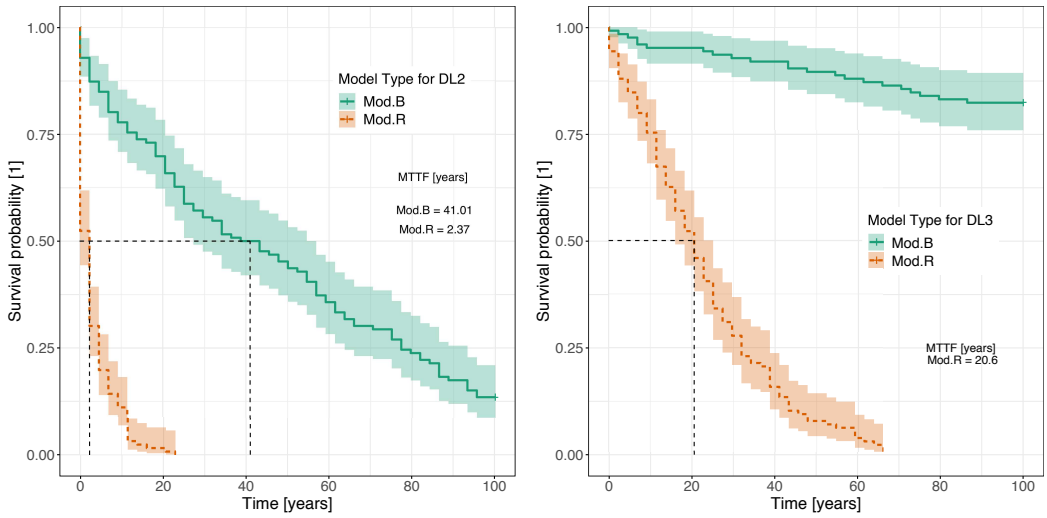

(a) (b)

Figure 14: The survival analysis of *Mod.B* in back-to-back form for a) DL2 and b) DL3

that the response varies with the ground motion model, which points on the importance of the choice of the stochastic method to generate the ground motions.

9. Conclusions

This paper presents the survival analysis of a liquefiable embankment subjected to sequential earthquakes. First, it started with a site-specific seismic analysis where the damage was quantified after a set of unsequenced ground motion records. To generalize this work, two synthetic ground motion models were used. They were extracted from the studies of Rezaeian and Der Kiureghian [45] and Boore [7] and were designated in this paper as *Mod.R* and *Mod.B* respectively. Then, one synthetic model (e.g. *Mod.R*) was chosen for the analysis. Sequential mainshocks were created accordingly, and the damage was calculated after each sequence. A total of 210 sequences composed of 44 acceleration time histories each, were generated in order to represent a lifetime of 100 years. Finally, the survival function and its corresponding Mean Time To Failure (MTTF) were calculated. For these purposes, an elastoplastic multi-mechanism soil behavior model was used with the help of a 2D finite element code (*GEFDyn*).

The conclusions that this paper have found are the following:

- For the site-specific seismic analysis, *Mod.R* showed a large variety of the response than *Mod.B*. The relative crest settlement of this model was mainly between *Minor* and *Moderate* damage levels.

- The cumulative damage in this study showed two responses for the embankment: i) a progressive deterioration that did not necessarily lead to drastic damages or ii) a sudden deterioration after few years.

- Based on the survival function, it was shown that after 25 years (MTTF = 25 years), the embankment have 50% chance to present *Moderate*

damage. Whereas it will not show *Serious* damage during its lifetime. These results prove that classical or short-term analysis are not always a good idea to know the global performance of the embankment.

- The distribution of the survival function for the *Moderate* damage level, follows a Weibull distribution whereas that of the *Serious* damage level is more likely to be represented by an exponential distribution. In addition, parameters of each distribution were calculated for each type of analysis.

- The consideration of the loading history for geo-structures is very important since the MTTF changed from 6 years to 25 years. In addition, a recovery time between each ground motion is essential in order to ensure the dissipation of the excess pore water pressure and it was shown in this study, that the MTTF is also affected.

- It is very important to pay attention to the chosen synthetic ground motion model since the performance might highly be affected. The MTTF for *Mod.B* was under estimated comparing to *Mod.R*.

It should be noted that the above conclusions are based on the results corresponding to soil behavior models and stochastic GM models adopted in this paper.

Acknowledgment

This work, within the ISOLATE project, benefited from French state funding managed by the National Research Agency reference under program

669 Mobility and Sustainable Urban Systems (DS06) 2017 reference No. ANR-
670 17-CE22-0009. The research reported in this paper has been supported in
671 part by the SEISM Paris Saclay Research Institute.

672 References

673 [1] Akkar, S., Sandikkaya, M., and Bommer, J. J. (2014). Empirical ground-
674 motion models for point-and extended-source crustal earthquake scenar-
675 ios in europe and the middle east. *Bulletin of earthquake engineering*,
676 12(1):359–387.

677 [2] Aristizábal, C., Bard, P.-Y., Beauval, C., and Gómez, J. (2018). Inte-
678 gration of site effects into probabilistic seismic hazard assessment (psha):
679 A comparison between two fully probabilistic methods on the euroseistest
680 site. *Geosciences*, 8(8):285.

681 [3] Aubry, D., Chouvet, D., Modaressi, A., and Modaressi, H. (1986). Gef-
682 dyn: Logiciel d'analyse de comportement mécanique des sols par éléments
683 finis avec prise en compte du couplage sol-eau-air. *Manuel scientifique,*
684 *Ecole Centrale Paris, LMSS-Mat.*

685 [4] Aubry, D., Hujeux, J., Lassoudiere, F., and Meimon, Y. (1982). A double
686 memory model with multiple mechanisms for cyclic soil behaviour. In
687 *Proceedings of the Int. Symp. Num. Mod. Geomech*, pages 3–13.

688 [5] Bazzurro, P. and Allin Cornell, C. (1999). Disaggregation of seismic
689 hazard. *Bulletin of the Seismological Society of America*, 89(2):501–520.

690 [6] Bommer, J. J. (2002). Deterministic vs. probabilistic seismic hazard as-
691 sessment: an exaggerated and obstructive dichotomy. *Journal of Earth-*
692 *quake Engineering*, 6(spec01):43–73.

693 [7] Boore, D. M. (1996). *SMSIM: Fortran programs for simulating ground*
694 *motions from earthquakes: Version 1.0*. Citeseer.

695 [8] Boore, D. M. (2003). Simulation of ground motion using the stochastic
696 method. *Pure and applied geophysics*, 160(3-4):635–676.

697 [9] Bradburn, M. J., Clark, T. G., Love, S., and Altman, D. (2003). Survival
698 analysis part ii: multivariate data analysis–an introduction to concepts
699 and methods. *British journal of cancer*, 89(3):431.

700 [10] Campbell, K. W. and Bozorgnia, Y. (2008). Nga ground motion model
701 for the geometric mean horizontal component of pga, pgv, pgd and 5%
702 damped linear elastic response spectra for periods ranging from 0.01 to 10
703 s. *Earthquake Spectra*, 24(1):139–171.

704 [11] Causse, M., Laurendeau, A., Perrault, M., Douglas, J., Bonilla, L. F.,
705 and Guéguen, P. (2014). Eurocode 8-compatible synthetic time-series as
706 input to dynamic analysis. *Bulletin of earthquake engineering*, 12(2):755–
707 768.

708 [12] Christodoulou, S. E. and Fragiadakis, M. (2014). Vulnerability assess-
709 ment of water distribution networks considering performance data. *Journal*
710 *of Infrastructure Systems*, 21(2):04014040.

711 [13] Clark, T., Bradburn, M., Love, S., and Altman, D. (2003). Survival

analysis part i: basic concepts and first analyses. *British journal of cancer*, 89(2):232.

[14] Di Sarno, L. and Pugliese, F. (2020). Seismic fragility of existing rc buildings with corroded bars under earthquake sequences. *Soil Dynamics and Earthquake Engineering*, 134:106169.

[15] Diamoutene, A., Barro, D., Somda, S. M. A., Noureddine, F., and Kamsu-Foguem, B. (2016). Survival analysis in living and engineering sciences.

[16] Eurocode, E. (1994). 1: 1995 basis of design and actions on structures–part 1: Basis of design.

[17] Ghosh, J., Padgett, J. E., and Sánchez-Silva, M. (2015). Seismic damage accumulation in highway bridges in earthquake-prone regions. *Earthquake Spectra*, 31(1):115–135.

[18] Goda, K. (2012). Nonlinear response potential of mainshock–aftershock sequences from japanese earthquakes. *Bulletin of the Seismological Society of America*, 102(5):2139–2156.

[19] Gomes, R. C., Santos, J. A., Modaressi-Farahmand-Razavi, A., and Lopez-Caballero, F. (2016). Validation of a strategy to predict secant shear modulus and damping of soils with an elastoplastic model. *KSCE Journal of Civil Engineering*, 20(2):609–622.

[20] Hatzigeorgiou, G. D. and Beskos, D. E. (2009). Inelastic displacement ratios for sdof structures subjected to repeated earthquakes. *Engineering Structures*, 31(11):2744–2755.

[21] Hosmer Jr, D. W. and Lemeshow, S. (1999). Applied survival analysis: regression modelling of time to event data (1999). *Eur Orthodontic Soc*, pages 561–2.

[22] Hosmer Jr, D. W., Lemeshow, S., and May, S. (2008). *Applied survival analysis: regression modeling of time-to-event data*, volume 618. Wiley-Interscience.

[23] Hu, S., Gardoni, P., and Xu, L. (2018). Stochastic procedure for the simulation of synthetic main shock-aftershock ground motion sequences. *Earthquake Engineering & Structural Dynamics*, 47(11):2275–2296.

[24] Iervolino, I., Chioccarelli, E., and Suzuki, A. (2020). Seismic damage accumulation in multiple mainshock–aftershock sequences. *Earthquake Engineering & Structural Dynamics*, 49(10).

[25] Iervolino, I., Giorgio, M., and Polidoro, B. (2015). Reliability of structures to earthquake clusters. *Bulletin of Earthquake Engineering*, 13(4):983–1002.

[26] Jungmeier, G., Hingsamer, M., Steiner, D., Kaltenegger, I., Kleinegris, D., van Ree, R., and de Jong, E. (2016). The approach of life cycle sustainability assessment of biorefineries. In *EUBCE 2016: 24th European Biomass Conference and Exibition*.

[27] Kaplan, E. L. and Meier, P. (1958). Nonparametric estimation from incomplete observations. *Journal of the American statistical association*, 53(282):457–481.

[28] Kartsonaki, C. (2016). Survival analysis. *Diagnostic Histopathology*, 22(7):263–270.

[29] Kawase, H. (2011). Strong motion characteristics and their damage impact to structures during the off pacific coast of tohoku earthquake of march 11, 2011: How extraordinary was this m9. 0 earthquake. In *Proceedings, 4th IASPEI/IAEE International Symposium*.

[30] Kramer, S. L. (1996). Geotechnical earthquake engineering. in prentice–hall international series in civil engineering and engineering mechanics. *Prentice-Hall, New Jersey*.

[31] Kuhl, D. and Crisfield, M. (1999). Energy-conserving and decaying algorithms in non-linear structural dynamics. *International journal for numerical methods in engineering*, 45(5):569–599.

[32] Lilliefors, H. W. (1967). On the kolmogorov-smirnov test for normality with mean and variance unknown. *Journal of the American statistical Association*, 62(318):399–402.

[33] Lopez-Caballero, F., Aristizabal, C., and Sanchez-Silva, M. (2020). A model to estimate the lifetime of structures located in seismically active regions. *Engineering Structures*, 215:110662.

[34] Lopez-Caballero, F. and Khalil, C. (2018). Vulnerability assessment for earthquake liquefaction–induced settlements of an embankment using gaussian processes. *ASCE-ASME Journal of Risk and Uncertainty in Engineering Systems, Part A: Civil Engineering*, 4(2):04018010.

[35] Lopez-Caballero, F., Modaressi-Farahmand-Razavi, A., and Modaressi, H. (2007). Nonlinear numerical method for earthquake site response analysis I - elastoplastic cyclic model and parameter identification strategy. *Bulletin of Earthquake Engineering*, 5(3):303–323.

[36] Lopez-Caballero, F., Modaressi-Farahmand-Razavi, A., and Stamatopoulos, C. A. (2016). Numerical evaluation of earthquake settlements of road embankments and mitigation by preloading. *International Journal of Geomechanics*, 16(5):C4015006.

[37] Luco, N. and Cornell, C. A. (2007). Structure-specific scalar intensity measures for near-source and ordinary earthquake ground motions. *Earthquake Spectra*, 23(2):357–392.

[38] Modaressi, H. and Benzenati, I. (1994). Paraxial approximation for poroelastic media. *Soil Dynamics and Earthquake Engineering*, 13(2):117–129.

[39] Nafday, A. M. (2010). Soil liquefaction modelling by survival analysis regression. *Georisk*, 4(2):77–92.

[40] Nakagawa, T. (2007). *Shock and damage models in reliability theory*. Springer Science & Business Media.

[41] Panchireddi, B. and Ghosh, J. (2019). Cumulative vulnerability assessment of highway bridges considering corrosion deterioration and repeated earthquake events. *Bulletin of earthquake engineering*, 17(3):1603–1638.

[42] Ranjkesh, S. H., Hamadani, A. Z., and Mahmoodi, S. (2019). A new

cumulative shock model with damage and inter-arrival time dependency. *Reliability Engineering & System Safety*, 192:106047.

[43] Rapti, I., Lopez-Caballero, F., Modaressi-Farahmand-Razavi, A., Foucault, A., and Voldoire, F. (2018). Liquefaction analysis and damage evaluation of embankment-type structures. *Acta Geotechnica*, pages 1–19.

[44] Rathje, E. M. and Saygili, G. (2011). Estimating fully probabilistic seismic sliding displacements of slopes from a pseudoprobabilistic approach. *Journal of geotechnical and geoenvironmental engineering*, 137(3):208–217.

[45] Rezaeian, S. and Der Kiureghian, A. (2012). Simulation of orthogonal horizontal ground motion components for specified earthquake and site characteristics. *Earthquake Engineering & Structural Dynamics*, 41(2):335–353.

[46] Riascos-Ochoa, J., Sánchez-Silva, M., and Klutke, G.-A. (2016). Modeling and reliability analysis of systems subject to multiple sources of degradation based on lévy processes. *Probabilistic Engineering Mechanics*, 45:164–176.

[47] Ruiz-García, J. (2012). Mainshock-aftershock ground motion features and their influence in building's seismic response. *Journal of Earthquake Engineering*, 16(5):719–737.

[48] Ruiz-García, J. (2014). Discussion on "effects of multiple earthquakes on inelastic structural response". *Engineering structures*, 58:110–111.

[49] Ruiz-Garcia, J. and Negrete-Manriquez, J. C. (2011). Evaluation of drift demands in existing steel frames under as-recorded far-field and near-fault

mainshock-aftershock seismic sequences. *Engineering Structures*, 33(2):621 – 634.

[50] Sáez, E., Lopez-Caballero, F., and Modaressi-Farahmand-Razavi, A. (2011). Effect of the inelastic dynamic soil–structure interaction on the seismic vulnerability assessment. *Structural safety*, 33(1):51–63.

[51] Salami, M. R., Kashani, M. M., and Goda, K. (2019). Influence of advanced structural modeling technique, mainshock-aftershock sequences, and ground-motion types on seismic fragility of low-rise rc structures. *Soil Dynamics and Earthquake Engineering*, 117:263–279.

[52] Sanchez-Silva, M., Klutke, G. A., and Rosowsky, D. V. (2011). Life-cycle performance of structures subject to multiple deterioration mechanisms. *Structural safety*, 33:206–217.

[53] Schober, P. and Vetter, T. R. (2018). Survival analysis and interpretation of time-to-event data: The tortoise and the hare. *Anesthesia and analgesia*, 127(3):792.

[54] Seyedi, D., Gehl, P., Douglas, J., Davenne, L., Mezher, N., and Ghavamian, S. (2010). Development of seismic fragility surfaces for reinforced concrete buildings by means of nonlinear time-history analysis. *Earthquake Engineering & Structural Dynamics*, 39(1):91–108.

[55] Shome, N. (1999). *Probabilistic seismic demand analysis of nonlinear structures*. Stanford University.

[56] Sica, S., Pagano, L., and Modaressi, A. (2008). Influence of past loading

history on the seismic response of earth dams. *Computers and Geotechnics*, 35(1):61–85.

[57] Stewart, J. P., Chiou, S.-J., Bray, J. D., Graves, R. W., Somerville, P. G., and Abrahamson, N. A. (2002). Ground motion evaluation procedures for performance-based design. *Soil dynamics and earthquake engineering*, 22(9-12):765–772.

[58] Swaisgood, J. (2003). Embankment dam deformations caused by earthquakes. In *PCEE 2003: 7th Pacific Conference on Earthquake Engineering, University of Canterbury, Christchurch, New Zealand, Conference Handbook*, page Paper 014. New Zealand Society for Earthquake Engineering.

[59] Vamvatsikos, D. and Cornell, C. A. (2002). Incremental dynamic analysis. *Earthquake Engineering & Structural Dynamics*, 31(3):491–514.

[60] Wang, Z., Zentner, I., and Zio, E. (2020). Accounting for Uncertainties of Magnitude- and Site-Related Parameters on Neural Network-Computed Ground-Motion Prediction Equations. *Bulletin of the Seismological Society of America*, 110(2):629–646.

[61] Yamamoto, Y. and Baker, J. W. (2013). Stochastic model for earthquake ground motion using wavelet packets. *Bulletin of the Seismological Society of America*, 103(6):3044–3056.

[62] Yeo, G. L. and Cornell, C. A. (2009). Building life-cycle cost analysis due to mainshock and aftershock occurrences. *Structural Safety*, 31(5):396–408.

[63] Zhai, C.-H., Wen, W.-P., Chen, Z., Li, S., and Xie, L.-L. (2013). Damage spectra for the mainshock–aftershock sequence-type ground motions. *Soil Dynamics and Earthquake Engineering*, 45:1–12.

[64] Zienkiewicz, C. (1991). The finite element method; solid adnd fluid mechanics. *Dynamics and non-linearity*, 2:219.